Met. Mater. Int., Vol. 23, No. 5 (2017), pp. 964~973
doi: 10.1007/s12540-017-6391-8

Kinetics and Critical Conditions for Initiation of Dynamic Recrystallization During Hot Compression Deformation of AISI 321 Austenitic Stainless Steel

Mehdi Shaban Ghazani[1], Beitallah Eghbali[1,*], and Gholamreza Ebrahimi[2]

[1]Department of Materials Science and Engineering, Sahand University of Technology, Tabriz 1996-51335, Iran.
[2]Department of Materials and Polymer Engineering, Hakim Sabzevari University, Sabzevar 9617976487, Iran.

(received date: 6 June 2016 / accepted date: 22 August 2016)

Dynamic recrystallization behavior of AISI 321 austenitic stainless steel were studied using hot compression tests over the range of temperatures from 900 °C to 1200 °C and strain rates from 0.001 s^{-1} to 1 s^{-1}. The critical strain and stress for initiation of dynamic recrystallization were determined by plotting strain hardening rate vs. stress curves and a constitutive equation describing the flow stress at strains lower than peak strain. Also, the strain at maximum flow softening was obtained and the effect of deformation conditions (Z parameter) on the critical strain and stress were analyzed. Finally, the volume fraction of dynamic recrystallization was calculated at different deformation conditions using these critical values. Results showed that the model used for predicting the kinetics of dynamic recrystallization has a great consistency with the data, in the form of θ-ε curves, directly acquired from experimental flow curves.

Keywords: metals, deformation, hot working, microstructure, recrystallization

1. INTRODUCTION

During high temperature deformation of materials softening may occur through dynamic recovery and/or dynamic recrystallization [1-3]. The occurrence of dynamic recrystallization has a major impact on the flow behavior of materials and results in the reduction of the rolling force in multi-stand deformation [4]. Also in multi pass hot rolling the occurrence of dynamic recrystallization alters the post dynamic softening mechanisms during inter-pass time and therefore affects the final microstructure and mechanical properties of the product [5-7]. So far, hot compression or torsion tests have usually been used for the simulation of high temperature response of metals and alloys [8-10]. The determination of critical strain for the onset of dynamic recrystallization in these experiments is of considerable importance because it demonstrates the occurrence of dynamic recrystallization [11,12]. Although the peak stress in the true stress versus true strain curves is an indication of the occurrence of dynamic recrystallization, but some alloys exhibit dynamic recrystallization without an obvious peak in the hot flow curves [13]. In addition, dynamic recrystallization occurs at strains lower than peak strain. But, the attainment of the critical stress (as well as the critical strain) does not reveal itself in the hot flow curve due to the smoothness of the stress variations before the peak strain [14]. Some researchers have proposed mathematical methods for determination of critical strain for the initiation of dynamic recrystallization. For example, Ryan and McQueen suggested that the onset of dynamic recrystallization can be identified by plotting strain hardening rate versus flow stress curves [15]. Also, Poliak and Jonas [16-18] have proposed the use of the minimum in the absolute value of the strain hardening slope which can be calculated from strain hardening rate versus flow stress curves. Inspection of literature data reveals that the initiation of dynamic recrystallization during hot deformation of Ti modified austenitic stainless steels has not been studied yet. Therefore, the aim of the present investigation is to determine the onset of dynamic recrystallization during hot compression deformation of AISI 321 austenitic stainless steel at different temperatures and strain rates. In addition, the strain at which dynamic softening rate reaches to its maximum value (ε^*) was determined by analyzing strain hardening rate versus strain curves and the calculated values were used to predict the kinetics of dynamic recrystallization.

2. EXPERIMENTAL PROCEDURE

The chemical composition of the AISI 321 austenitic stainless steel used in the present study was 0.042C, 0.365Si, 1.87Mn,

*Corresponding author: eghbali@sut.ac.ir

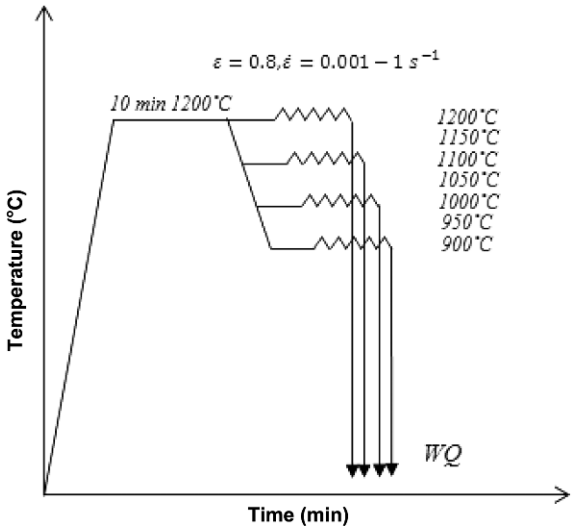

Fig. 1. Schematic of thermo-mechanical processing schedule conducted in the present study.

18.16Cr, 10.52Ni, 0.248Mo, 0.321Ti, and balance Fe. Hot compression samples in the form of cylinders with 15 mm length and 10 mm diameter were machined from as received rode. Specimens were then heated to 1200 °C for 10 min to achieve equiaxed austenite grain structure just before deformation. Hot compression tests were conducted isothermally in the temperature range of 900-1200 °C and strain rates of 0.001-1 s^{-1} using Zewick-Roell Z250 testing machine. Samples were water quenched immediately after a specified amount of plastic strain ($\varepsilon = 0.8$) to retain high temperature microstructure of material at ambient temperature. Figure 1 illustrates the schematic of thermo-mechanical processing schedule conducted in the present study. After imposing plastic deformation, samples were cut in to two halves and optical micrographs were taken from the center point of each sample. For this reason, the surface of deformed samples was sandpapered using 100-2500 grit in a standard manner. Afterwards, mechanical polishing was done using 0.05 micron Al_2O_3. Polished surfaces were electro-etched in a solution composed of 50% nitric acid and 50% distilled water by adopting current density to 0.3 A/cm^2 and microstructural observations performed using Olympus PMG3 optical microscope.

3. RESULTS AND DISCUSSIONS

3.1. Analysis of hot flow curves

The load-displacement data acquired from isothermal hot compression tests were converted to true stress-true strain curves. Figure 2 represents the true stress-true strain curves for AISI 321 austenitic stainless steel obtained at temperature range of 950-1200 °C and strain rates of 0.001-1 s^{-1}. As it is seen, the evolution of the most of flow curves follows the same trend and these curves indicate that AISI 321 austenitic stainless steel undergoes a typical dynamic recrystallization during deformation at high temperatures and low strain rates. In the initial stage of deformation process, the flow stress increases rapidly due to work hardening, caused by dislocation generation, and then reaches to a peak value. The peak in the stress-strain curves represents a balance between work hardening processes and softening due to dynamic recrystallization. Therefore, presence of peak in the hot flow curves is the major indication of the occurrence of dynamic recrystallization. After a peak stress, the flow stress decreases monotonically to a steady state value at higher strains. The difference between peak and steady state stresses (σ_p-σ_{ss}) reflects the kinetics of dynamic recrystallization. Therefore, the higher amounts of difference between these two parameters indicate that the kinetic of dynamic recrystallization is high enough to compensate the effect of work hardening and moreover soften material to a lower flow stress levels. By analyzing flow curves in Fig. 2, it is deduced that the difference between peak and steady state stresses (σ_p-σ_{ss}), and therefore the kinetics of dynamic recrystallization decreases by increasing strain rate and lowering deformation temperature. This is due to the fact that dynamic recrystallization is a thermal activated metallurgical phenomenon and occurs through nucleation and growth mechanisms. Grain boundary mobility is increased by increasing deformation temperature [19]. Therefore, the growth of dislocation free grains is accelerated by increasing deformation temperature. Also, the time required for completion of deformation process is decreased by increasing strain rate and this limits the extent of grain growth after nucleation. It can be seen in Fig. 2 that the stress strain curves of AISI 321 austenitic stainless steel deformed at 950 °C and 1000 °C with strain rate of 1 s^{-1}, show a trend similar to dynamic recovery where the stress level remains constant after a specified amount of deformation. So that, the occurrence of dynamic recrystallization is not expected for these conditions by observing obtained flow curves. Whereas, the microstructural observations reveal that dynamic recrystallization occurs at these deformation conditions. Figure 3 shows optical microstructures of samples deformed at 950 °C and 1000 °C with strain rate of 1 s^{-1}. The existence of equi-axed austenite grains in these micrographs approves the initiation of dynamic recrystallization during hot compression deformation.

3.2. Deformation activation energy

The Arrhenius type equation is most widely used for constitutive description of the hot flow behavior of materials [20]. This equation relates flow stress to hot deformation parameters, including temperature and strain rate, as below:

$$Z = \dot{\varepsilon}\exp\left(\frac{Q}{RT}\right) = A[\sinh(\alpha\sigma)]^n \quad (1)$$

where $\dot{\varepsilon}$ is strain rate, T is deformation temperature, Q is defamation activation energy, R is universal gas constant, σ

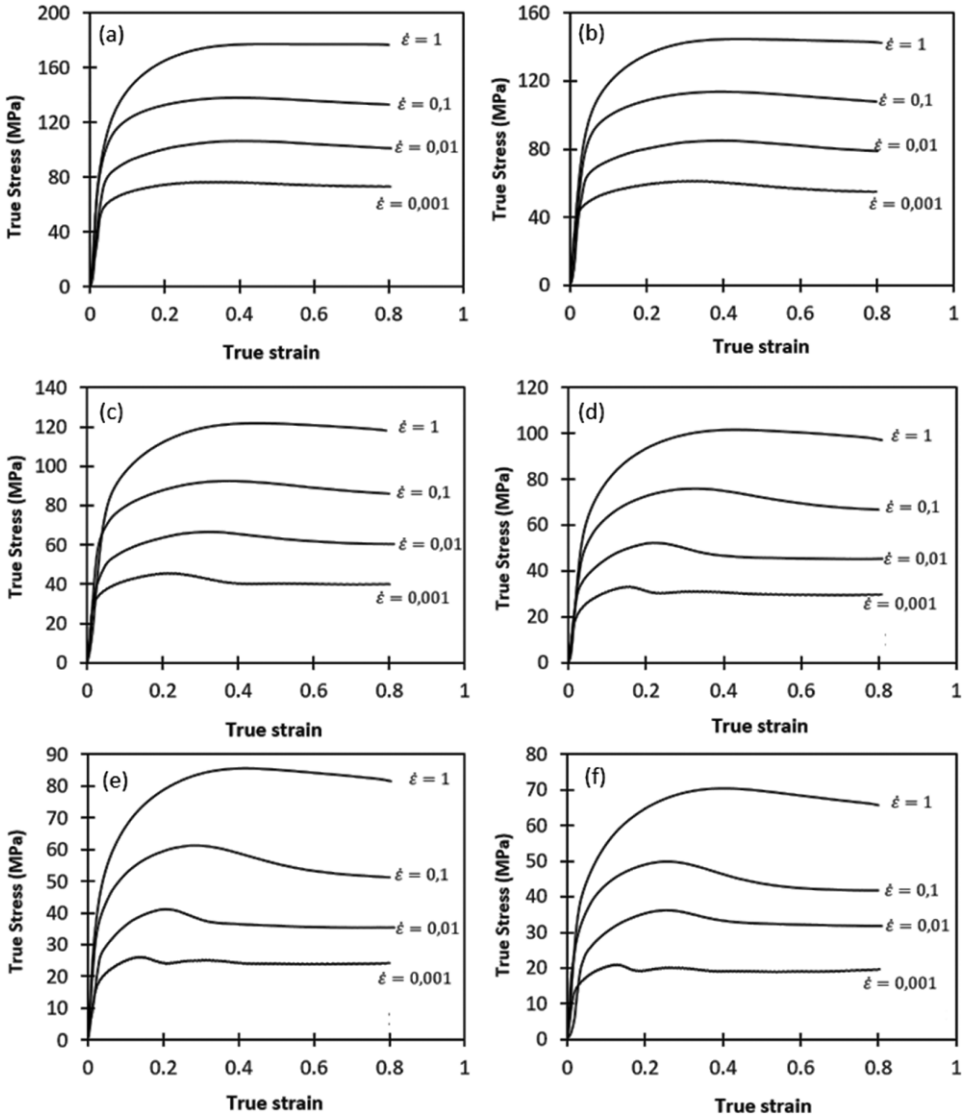

Fig. 2. Hot compression flow curves of AISI 321 austenitic stainless steel deformed at different temperatures and strain rates: (a) 950 °C, (b) 1000 °C, (c) 1050 °C, (d) 1100 °C, (e) 1150 °C, and (f) 1200 °C.

is flow stress and A, n and α are material constants. By taking a natural logarithm from the both sides of Eq. 1 the following expression is obtained:

$$\ln Z = \ln\dot{\varepsilon} + \frac{Q}{RT} = \ln A + n\ln[\sinh(\alpha\sigma)] \quad (2)$$

According to the procedure described elsewhere [21], the values of constants A, α, n were calculated to be 1.148×10^{16}, 0.013 and 5.07 respectively. Considering Eq. 2, deformation activation energy can be defined as below:

$$Q = nR\left[\frac{\delta(\ln[\sinh(\alpha\sigma)])}{\delta\left(\frac{1}{T}\right)}\right]_{\dot{\varepsilon}=constant} \quad (3)$$

Figure 4 shows $\ln[\sinh(\alpha\sigma)]$ versus (1/T) curves at constant strain rate. The average slope of these curves were determined and then used for calculation of deformation activation energy (Q = Slop × n × R). The resultant value was about 444 kJ/mol.

3.3. Initiation of dynamic recrystallization

3.3.1. Strain hardening rate vs. stress curves

As mentioned before, the onset of dynamic recrystallization does not reveal itself in hot flow curves of materials and the lack of peak stress could not be attributed only to occurrence of dynamic recovery. In the alternative method proposed by Poliak and Jonas [17] the plots of strain hardening rate ($\theta = d\sigma/ds$) as a function of flow stress (σ) are used to calculate critical stress and strain for the initiation of dynamic recrystallization. Figure 5 represents the calculated θ-σ plots for the hot flow curves given in Fig. 2. The inflection point

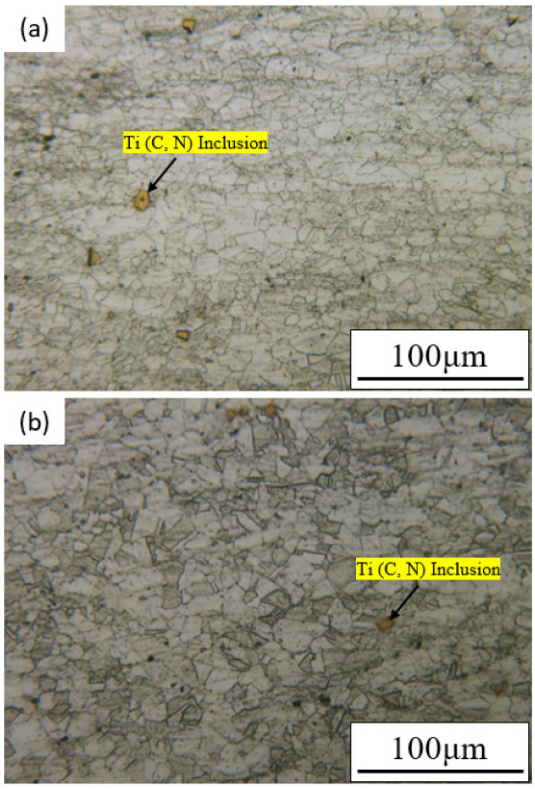

Fig. 3. Optical microstructure of AISI 321 stainless steel deformed at different temperatures: (a) 950 °C and (b) 1000 °C with constant strain rate of 1 s^{-1}.

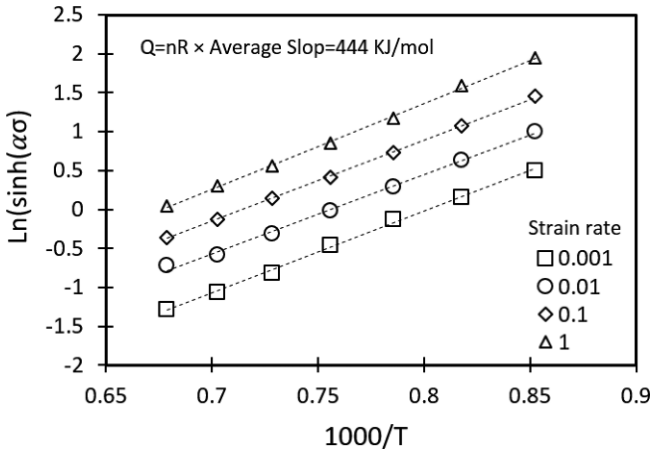

Fig. 4. The plot of Ln (sinh (ασ)) versus (1/T) for calculation of deformation activation energy.

in the θ-σ plots corresponds to critical stress. Using the data given in Fig. 5, the derivatives of the strain hardening rate ($\theta = d\sigma/d\varepsilon$) as a function of flow stress (σ) were calculated for various deformation temperatures and strain rates. The obtained $d\theta/d\sigma$ vs. σ plots are shown in Fig. 6. As it is seen, the maximum points in these curves represent the critical stress. In addition, the critical strain for the initiation of dynamic recrystallization (ε_c) can be defined by mapping the critical stress back into stress-strain curves. Figure 7 shows the θ-σ plots for the hot flow curves obtained at deformation temperatures of 950 °C and 1000 °C and strain rate of 1 s^{-1}. As it is evident, the inflection points are also seen in these plots irrespective of the dynamic recovery type of the flow curves which previously observed at these conditions (Fig. 2). Therefore, the existence of inflection point in the θ vs. σ or a maximum point in the $d\theta/d\sigma$ vs. σ plots is a definite evidence for the initiation of dynamic recrystallization during hot deformation of materials. By inspection of Fig. 5 and Fig. 6 it is concluded that the values of critical stress and strain are increased by increasing strain rate and decreasing deformation temperature. It is worth noting that during deformation of low stacking fault energy materials up to critical strain, work hardening and recovery lead to a development of a dislocation subgrain structure, but dislocations in the subgrain boundaries remain tangled, rather than forming the clean two dimensional networks observed in metals in which recovery is more rapid. The existence of these higher energy tangled subgrain boundaries is essential to obtain sufficient stored energy differences in local regions to nucleate dynamic recrystallization. Therefore, the increase of critical strain and stress with increasing strain rate and decreasing deformation temperature result from the need for increasing stored energy difference in two sides of moving boundary to ensure that boundary migration is sufficiently rapid for growth of the nuclei before the dislocation density behind the moving boundary has been increased by concurrent deformation to destroy the initial driving force [22]. Dependence of critical strain and stress on deformation conditions (Zener-Hollomon parameter) is depicted in Fig. 8. As it is seen, calculated values of critical strain and stress are increased by increasing Z parameter. So that, the following equations are derived to express the relationship between these critical values and Z parameter based on Poliak and Jonas method:

$$\varepsilon_c = 0.0139\ Z^{0.0686} \tag{4}$$

$$\sigma_c = 0.3426\ Z^{0.144} \tag{5}$$

3.3.2. Modeling of critical strain

The hot flow curves of materials up to the peak strain (ε_p) can be modeled using the equation as shown below [23]:

$$\frac{\sigma}{\sigma_p} = \left[\left(\frac{\varepsilon}{\varepsilon_p}\right)\exp\left(1-\frac{\varepsilon}{\varepsilon_p}\right)\right]^c \tag{6}$$

where σ is flow stress, ε is true strain, σ_p is peak stress, ε_p is peak strain and C is a constant. By taking a natural logarithm from the both side of this equation the following expression is obtained:

$$\ln\left(\frac{\sigma}{\sigma_p}\right) = c\left[\ln\left(\frac{\varepsilon}{\varepsilon_p}\right)+\left(1-\frac{\varepsilon}{\varepsilon_p}\right)\right] \tag{7}$$

Therefore, the plots of $\ln(\sigma/\sigma_p)$ vs. $\ln(\varepsilon/\varepsilon_p) + (1-\varepsilon/\varepsilon_p)$ are

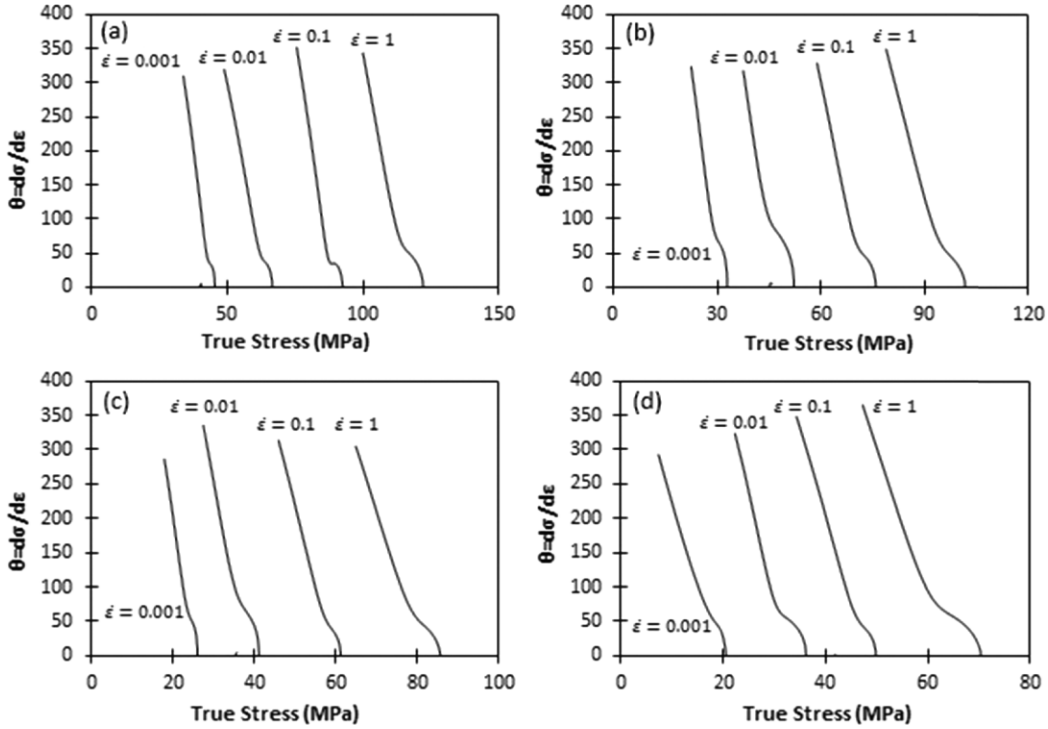

Fig. 5. Calculated θ-σ curves of hot deformed AISI 321 austenitic stainless steel at different temperatures and strain rates: (a) 1050 °C, (b) 1100 °C, (c) 1150 °C, and (d) 1200 °C.

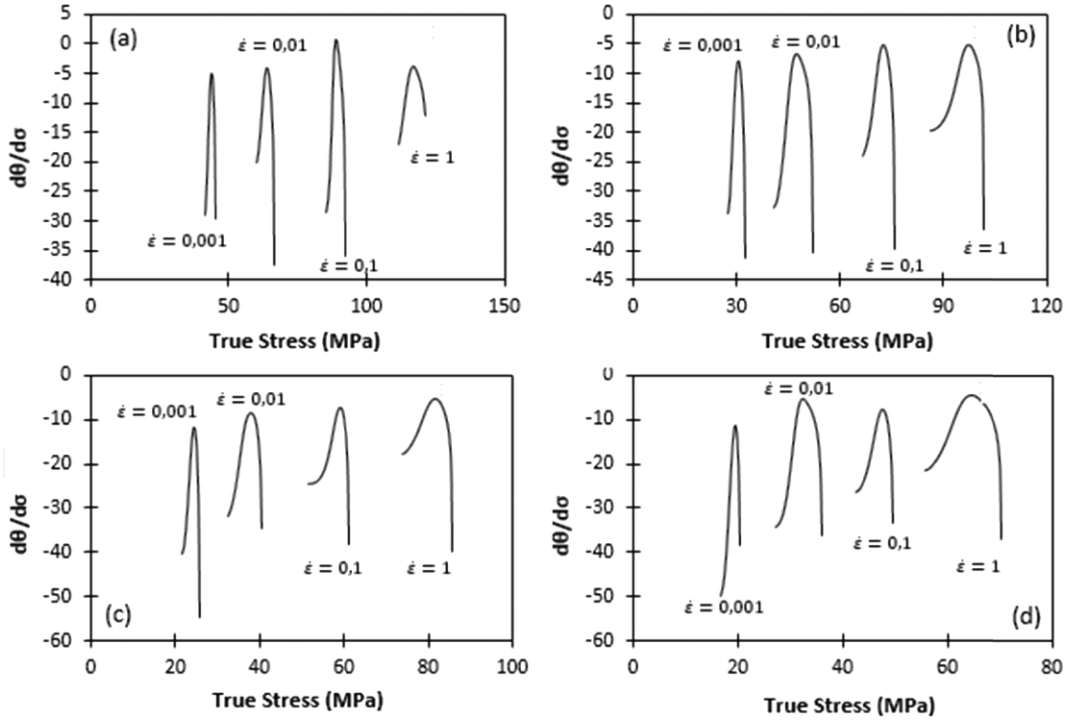

Fig. 6. Calculated dθ-dσ curves of hot deformed AISI 321 austenitic stainless steel at different temperatures and strain rates: (a) 1050 °C, (b) 1100 °C, (c) 1150 °C, and (d) 1200 °C.

used to calculate average values of C constants (in Eq. 6) at different deformation temperatures and strain rates. Examples of these calculations are shown in Fig. 9. According to Eq. 7, the slope of these linear curves gives the average value of constant C. As it is seen the value of constant C is calculated to be 0.5036 and 0.5511 for deformation temperature

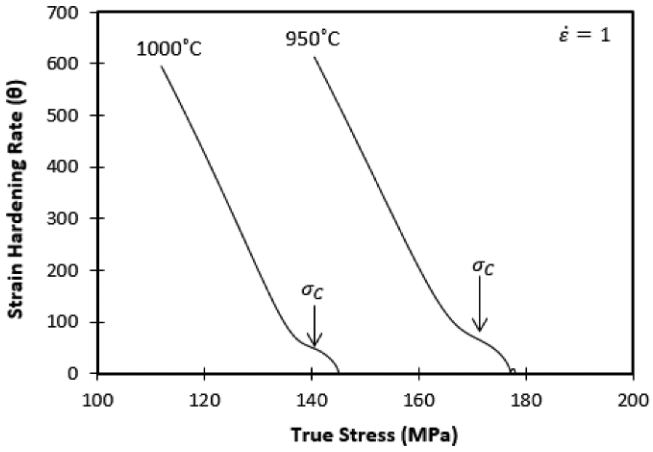

Fig. 7. θ-σ curves of hot deformed AISI 321 austenitic stainless steel deformed at 950 °C and 1000 °C with strain rate of 1 s^{-1}.

of 1200 °C and strain rates of 0.1 and 0.001 s^{-1} respectively. The work hardening rate (θ) of hot flow curves is a derivative of flow stress with respect to strain. Therefore, the following equation is obtained for θ by taking differentiate from Eq. 6:

$$\theta = \frac{d\sigma}{d\varepsilon} = C\sigma_p\left(\frac{1}{\varepsilon} - \frac{1}{\varepsilon_p}\right)\left[\left(\frac{\varepsilon}{\varepsilon_p}\right)\exp\left(1 - \frac{\varepsilon}{\varepsilon_p}\right)\right] \quad (8)$$

Knowing that the second derivative of θ with respect to ε is zero just at critical strain, the following equation is derived [24]:

$$\frac{\varepsilon_C}{\varepsilon_p} = \frac{\sqrt{1-C} - (1-C)}{C} \quad (9)$$

So that, the value of critical strain is obtained by substituting C and ε_p in to Eq. 9 which were calculated directly from hot flow curves. The dependence of modeled critical values on Z parameter is shown in Fig. 10. Following equations are derived to express the relationship between modeled values (critical stress and strain) and Z parameter:

$$\varepsilon_c = 0.004\ Z^{0.0927} \quad (10)$$

$$\sigma_c = 0.1748\ Z^{0.1615} \quad (11)$$

It is deduced, by inspection of Fig. 8 and Fig. 10, that the

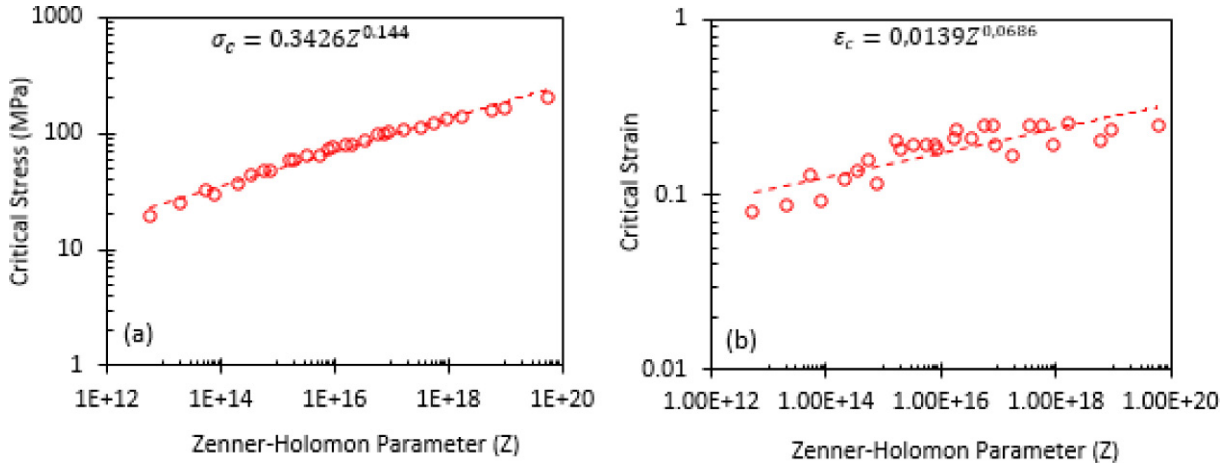

Fig. 8. Dependence of calculated critical stress (a), and critical strain (b) on Z parameter.

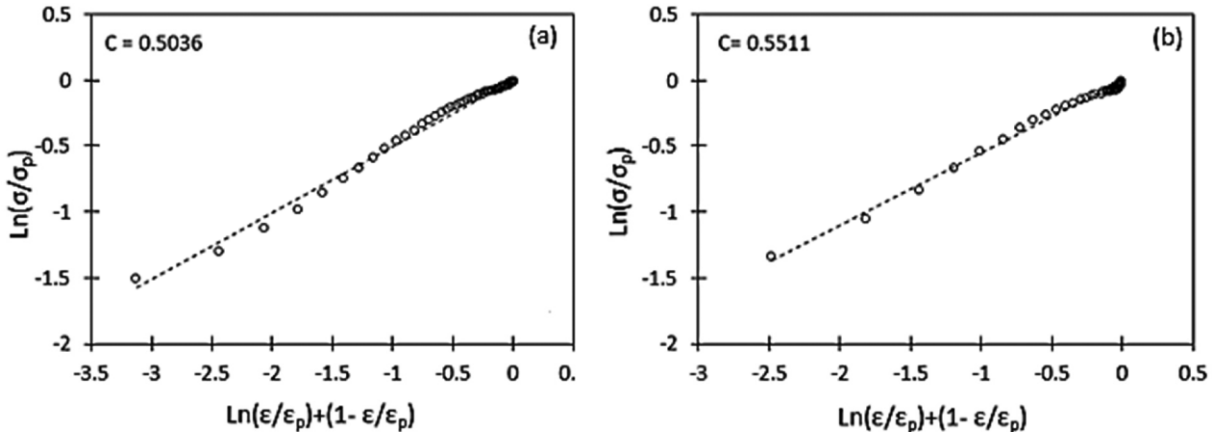

Fig. 9. Plots of ln(σ/σp) vs. ln(ε/εp)+(1- ε/εp) for calculation of C constant: (a) 1200 °C-0.1 s^{-1} and (b) 1200 °C-0.001 s^{-1}.

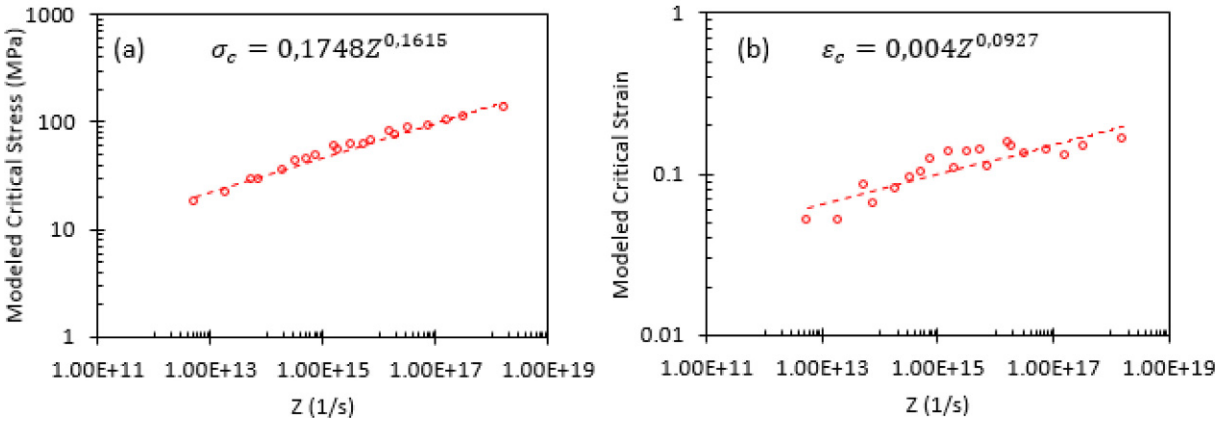

Fig. 10. The dependence of modeled critical stress (a) and modeled critical strain (b) on Z parameter.

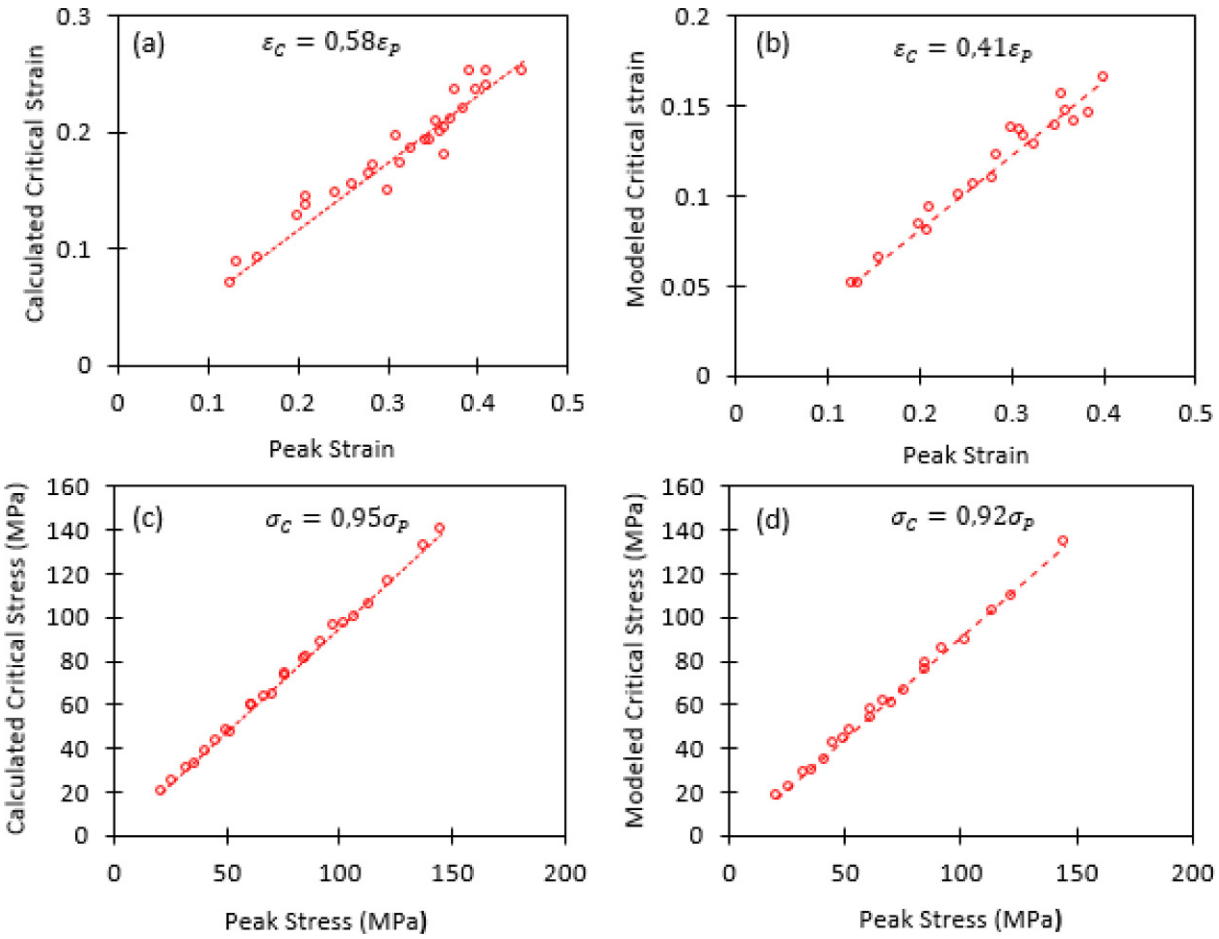

Fig. 11. The relationship between calculated and modeled critical strains (a and b) and peak strain, and the relationship between calculated and modeled critical stresses (c and d) and peak stress.

proposed model leads to lower values for both critical strain and stress compared with the result of direct measurement using Poliak and Jonas method.

3.3.3. Dependence of ε_c on ε_p and σ_c on σ_p

For modeling purposes, it is important to be able to express the quantities of critical strain and stress as a ratio of peak strain and stress respectively. The dependence of calculated and modeled values for critical strains and stresses on peak strain and stress is depicted in Fig. 11. The following expressions give a good fit to the data represented in these figures:

$$\sigma_C(Calculated) = 0.95\sigma_p \quad (12)$$

$$\sigma_C(Modeled) = 0.92\sigma_p \quad (13)$$

$$\varepsilon_C(Calculated) = 0.58\varepsilon_p \quad (14)$$

$$\varepsilon_C(Modeled) = 0.41\varepsilon_p \quad (15)$$

Obtained relationships between critical and peak values are in good agreement with those reported for other steels [25-27]. Also, by inspection of Eq. 9, it is concluded that the value of constant C must be in the range of 0 to 1. So that, the maximum value of 0.5 could be determined for $\varepsilon_c/\varepsilon_p$ using this model. Therefore, this model has a limitation and cannot be used for prediction of normalized strain values higher than 0.5.

3.4. Strain at maximum flow softening rate (ε*)

During plastic deformation of materials at high temperatures, the strain hardening rate is decreases gradually by increasing strain. This is due to the acceleration of the rate of dynamic recovery and also the onset of dynamic recrystallization. The occurrence of dynamic recrystallization at critical strain (ε_c) increases the softening rate and consequently the value of strain hardening rate (θ) reaches to zero at peak strain (ε_p). Beyond the peak strain, overall softening rate increases gradually and reaches to a maximum value at a specified strain (ε*). The value of ε* could be determined directly from strain hardening rate vs. strain curves (θ-ε). It is worth noting that the strain value at a maximum softening rate (ε*) is of considerable importance because the kinetics of dynamic recrystallization can be expressed with an Avrami type equation involving ε*. Figure 12 shows the obtained θ-ε curves at different temperatures and strain rates. As can be seen, the minimum points in these curves represent the value of ε*. The variation of the value of ε* with Z parameter is shown in Fig. 13. As it is seen, the ε* increases with increasing Z parameter. The relationship between ε* and Z parameter can be written as follow:

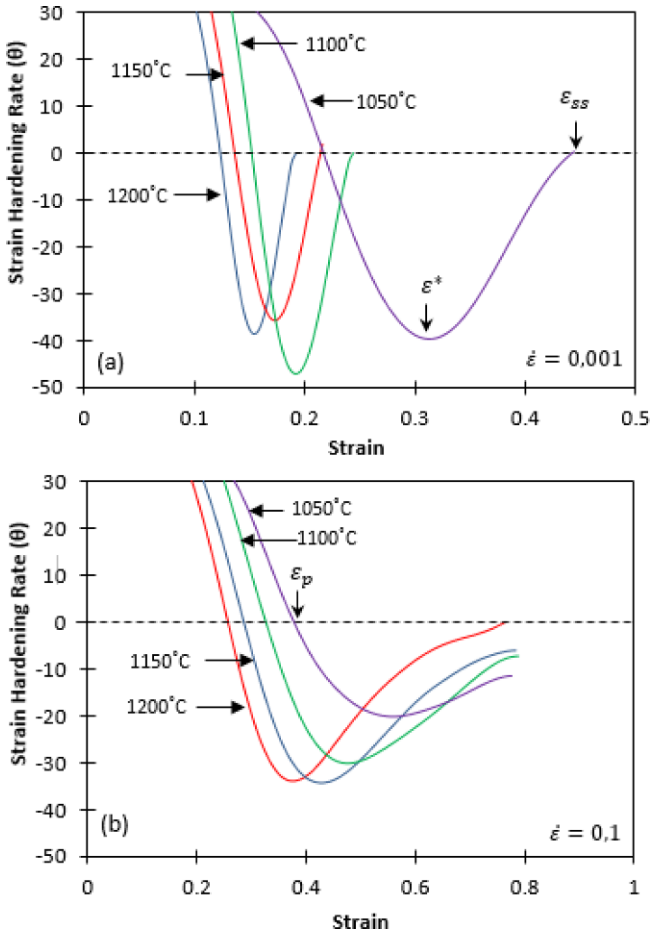

Fig. 12. Strain hardening rate vs. strain plots at different temperatures with strain rates of: (a) 0.001 s^{-1} and (b) 0.1 s^{-1}.

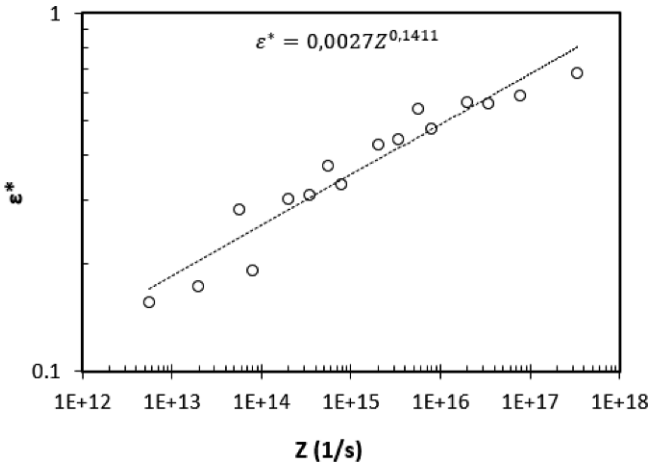

Fig. 13. Dependence of the value of ε* on Z parameter.

$$\varepsilon^* = 0.0027\ Z^{0.1411} \quad (16)$$

3.5. Dynamic recrystallization kinetics

The kinetics of dynamic recrystallization can be described using Avrami type equations. One of the most important expressions that relate the volume fraction of dynamic recrystallization to plastic strain is as follow [28]:

$$X_{DRX} = 1 - \exp\left[-0.693\left(\frac{\varepsilon - \varepsilon_c}{\varepsilon^* - \varepsilon_c}\right)^2\right] \quad (17)$$

where X_{DRX} is dynamic recrystallized volume fraction, ε is plastic strain, ε_c is critical strain for the onset of dynamic recrystallization and ε* is the strain in which the softening rate reaches to a maximum value during deformation. Figure 14 (a) shows the predicted values for the variations of the volume fraction of dynamic recrystallization with respect to plastic strain at constant temperature of 1150 °C and different strain rates. As it is seen, the dynamic recrystallized volume fraction increases with strain and reaches to a 100% after a specified amount of strain (when the steady state flow is initiated). Also,

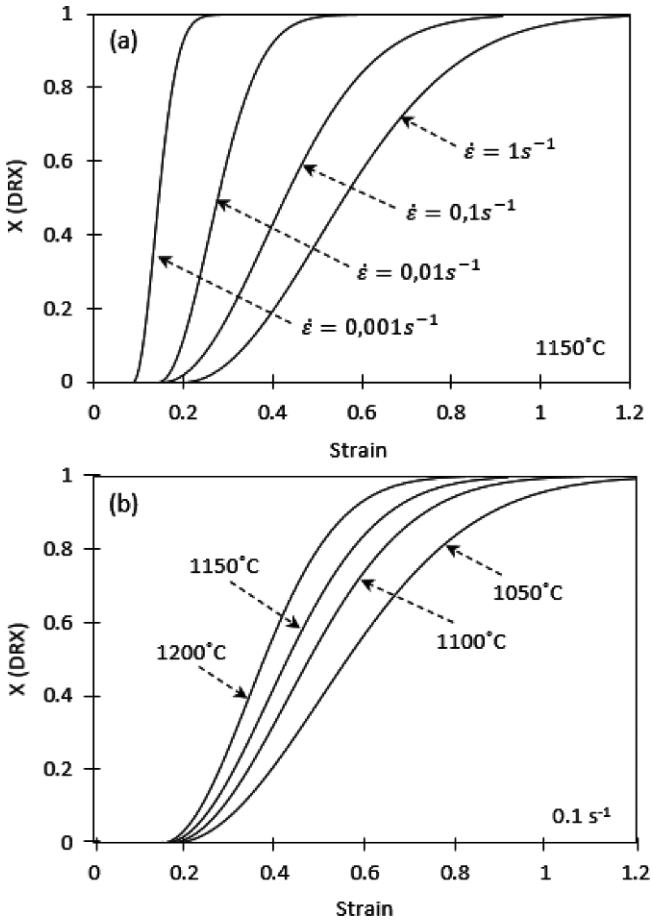

Fig. 14. Predicted volume fraction of recrystallization as a function of strain: (a) deformation at 1150 °C and different strain rates, (b) deformation at strain rate of 0.1 s^{-1} and different temperatures.

the plastic strain required for the same amounts of recrystallized fraction at different deformation conditions, is increased with increasing strain rate. In addition, the effect of deformation temperature on the kinetics of dynamic recrystallization is represented in Fig. 14(b). As can be seen, increasing deformation temperature accelerates the kinetics of dynamic recrystallization that is in contrast with the effect of increasing strain rate. The accuracy of the utilized equation can be verified by comparing strain hardening rate vs. strain curves (θ-ε) with X_{DRX} vs. strain curves (X_{DRX}-ε). In the θ-ε curves, the completion of dynamic recrystallization is identified by a second point at which the strain hardening rate becomes zero ($\theta = d\sigma/d\varepsilon = 0$, Fig. 12(b)). It is worth nothing that the first point with zero strain hardening rate denotes the peak strain in the hot flow curves of materials. In Fig. 15, the variations of the predicted volume fraction of recrystallization and work hardening rate are both plotted against strain. As it is seen, the onset of steady state deformation which is identified using θ-ε curve (second point with zero strain hardening rate) coincide with the completion of dynamic recrystallization ($X_{DRX} > 95\%$) which is predicted by the use of Avrami type equation.

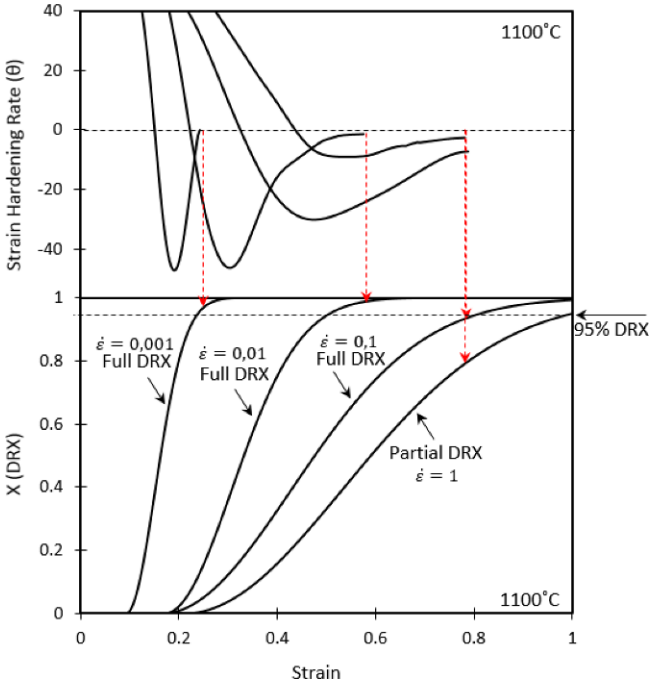

Fig. 15. Coincidence of the predicted steady strain using strain hardening rate vs. strain curve (θ = 0) and the method used for the calculation of dynamic recrystallization volume fraction ($X_{DRX} > 95\%$).

4. CONCLUSIONS

From the studies of dynamic recrystallization process in hot deformed AISI 321 austenitic stainless steel in the temperature range of 900-1200 °C and strain rates between 0.001 and 1 s^{-1}, following conclusions are made:

(1) Hot flow curves at deformation temperatures higher than 1050 °C shows a general trend of dynamic recrystallization at all applied strain rates. Whereas, the hot flow stress at 950 °C and 1000 °C and strain rate of 1 s^{-1} remains constant after a specified amount of plastic deformation as a flow curves obtained during dynamic recovery.

(2) Microstructural observations demonstrate the occurrence of dynamic recrystallization at 950 °C and 1000 °C irrespective of the DRV type of flow curves at these conditions.

(3) Hot deformation activation energy of AISI 321 austenitic stainless steel were calculated to be 444 kJ/mol in the temperature range of 900-1200 °C based on the Arrhenius modeling of flow curves.

(4) The critical stress and strain for the onset of dynamic recrystallization were determined using strain hardening rate vs. stress curves (θ-σ). The inflection point at these curves corresponds to critical stress. It is also concluded that these critical parameters are increased with increasing strain rate and decreasing deformation temperature. Following expressions were obtained for these critical parameters:

$$\varepsilon_c = 0.0139\, Z^{0.0686} \qquad \sigma_c = 0.3426\, Z^{0.144}$$

(5) The values for critical strain and stress obtained from modeling of flow curves before peak strain are lower than those calculated directly from θ-σ curves. This model gives the following expressions:

$$\varepsilon_c = 0.004\ Z^{0.0927} \qquad \sigma_c = 0.1748\ Z^{0.1615}$$

(6) Strain at maximum flow softening rate (ε*) is calculated at different temperatures and strain rates using θ-ε curves. Minimum point at these curves corresponds to ε*. This parameter is also a function of Zener-Hollomon parameter as bellow:

$$\varepsilon^* = 0.0027\ Z^{0.1411}$$

(7) Determination of dynamic recrystallization kinetics using critical strain (ε_c) and strain at maximum flow softening rate (ε*) gives a good estimation which is comparable with data acquired directly from hot flow curves.

REFERENCES

1. S. Kim and Y. Yoo, *Mat. Sci. Eng. A* **311**, 108 (2001).
2. A. I. Fernandez, P. Uranga, B. Lopez, and J. M. Rodriguez, *Mat. Sci. Eng. A* **361**, 367 (2003).
3. H. E. Hu, L. Zhen, B. Y. Zhang, L. Yang, and J. Z. Chen, *Mater. Charact.* **59**, 1185 (2008).
4. F. H. Samuel, S. Yue, J. J. Jonas, and B. A. Zbinden, *ISIJ Int.* **29**, 878 (1989).
5. C. Roucoules, P. D. Hodgson, S. Yue, and J. J. Jonas, *Metall. Mater. Trans. A* **25**, 389 (1994).
6. H. Beladi, P. Cizek, and P. D. Hodgson, *Scripta Mater.* **62**, 191 (2010).
7. P. Uranga, A. I. Fernandez, B. Lopez, and J. M. Rodriguez, *Mat. Sci. Eng. A* **345**, 319 (2003).
8. K. H. Jung, H. W. Lee, and Y. T. Lm, *Mat. Sci. Eng. A* **519**, 94 (2009).
9. M. Meysami and S. Mousavi, *Mat. Sci. Eng. A* **528**, 3049 (2011).
10. S. L. Semiatin and G. D. Lahoti, *Metall. Mater. Trans. A* **12**, 1719 (1981).
11. I. Mejia, A. Bedolla, C. Maldonado, and J. M. Cabrera, *Mat. Sci. Eng. A* **528**, 4133 (2011).
12. S. Solhjoo, *Mater. Design* **31**, 1360 (2010).
13. A. Dehghan-Manshadi, M. R. Barnet, and P. D. Hodgson, *Metall. Mater. Trans. A* **39**, 1359 (2008).
14. J. J. Jonas and E. I. Poliak, *Mater. Sci. Forum* **426-432**, 57 (2003).
15. N. D. Ryan and H. J. McQeen, *Can. Metall. Quart.* **29**, 147 (1990).
16. E. I. Poliak and J. J. Jonas, *ISIJ Int.* **43**, 684 (2003).
17. E. I. Poliak and J. J. Jonas, *Acta Mater.* **44**, 127 (1996).
18. E. I. Poliak and J. J. Jonas, *ISIJ Int.* **43**, 692 (2003).
19. P. R. Rios, F. S. Jr, H. R. Sandim, R. L. Plaut, and A. F. Padilha, *Mat. Res.* **8**, 225 (2005).
20. Y. C. Lin and X. Chen, *Mater. Design* **32**, 1733 (2011).
21. C. Sun, G. Liu, Q. Zhang, R. Li, and L. Wang, *Mat. Sci. Eng. A* **595**, 92 (2014).
22. C. M. Sellars, *Philos. T. R. Soc. A* **288**, 147 (1978).
23. R. Ebrahimi, S. H. Zahiri, and A. Najafizadeh, *J. Mater. Process. Tech.* **171**, 301 (2006).
24. H. Mirzadeh and A. Najafizadeh, *Mater. Design* **31**, 1174 (2010).
25. X. Liu, L. Zhang, R. Qi, L. Chen, M. Jin, and B. Guo, *J. Iron Steel Res. Int.* **23**, 238 (2016).
26. M. Shaban and B. Eghbali, *Mat. Sci. Eng. A* **527**, 4320 (2010).
27. A. D. Manshadi, M. R. Barnett, and P. D. Hodgson, *Mat. Sci. Eng. A* **485**, 664 (2008).
28. G. R. Stewart, A. M. Elwazri, S. Yue, and J. J. Jonas, *Mater. Sci. Tech.* **22**, 519 (2006).